Supporting Information

First Tandem Repeat of a Potassium Channel *KCNN4* Minisatellite Folds into a V-Loop G-Quadruplex Structure

Yoanes Maria Vianney and Klaus Weisz*

Institute of Biochemistry, Universität Greifswald, Felix-Hausdorff-Str. 4, D-17487 Greifswald, Germany

*Corresponding author: weisz@uni-greifswald.de

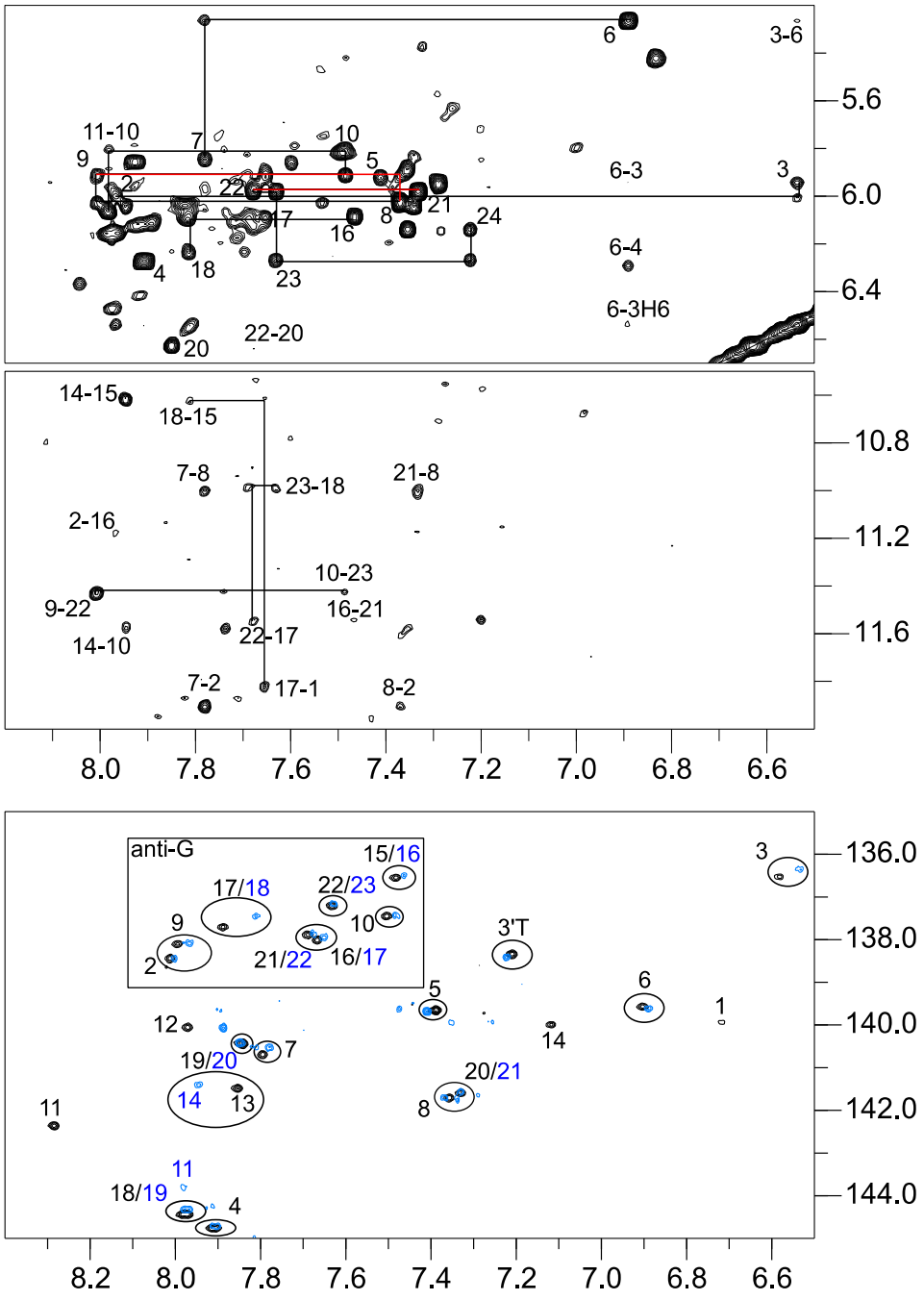

Figure S1. Partial assignment of *KNA-T*; 2D NOESY spectral region showing H6/8(ω_2)-H1'(ω_1) (top) and H6/8(ω_2)-H1(ω_1) cross-peaks (middle). Superimposed ^{1}H-^{13}C HSQC spectra with H6/8-C6/8 correlations of *KNA-ΔG13-T* (black, 0.9 mM) and *KNA-T* (blue) (bottom); overlapping cross-peaks and cross-peak patterns suggest identical G4 topologies.

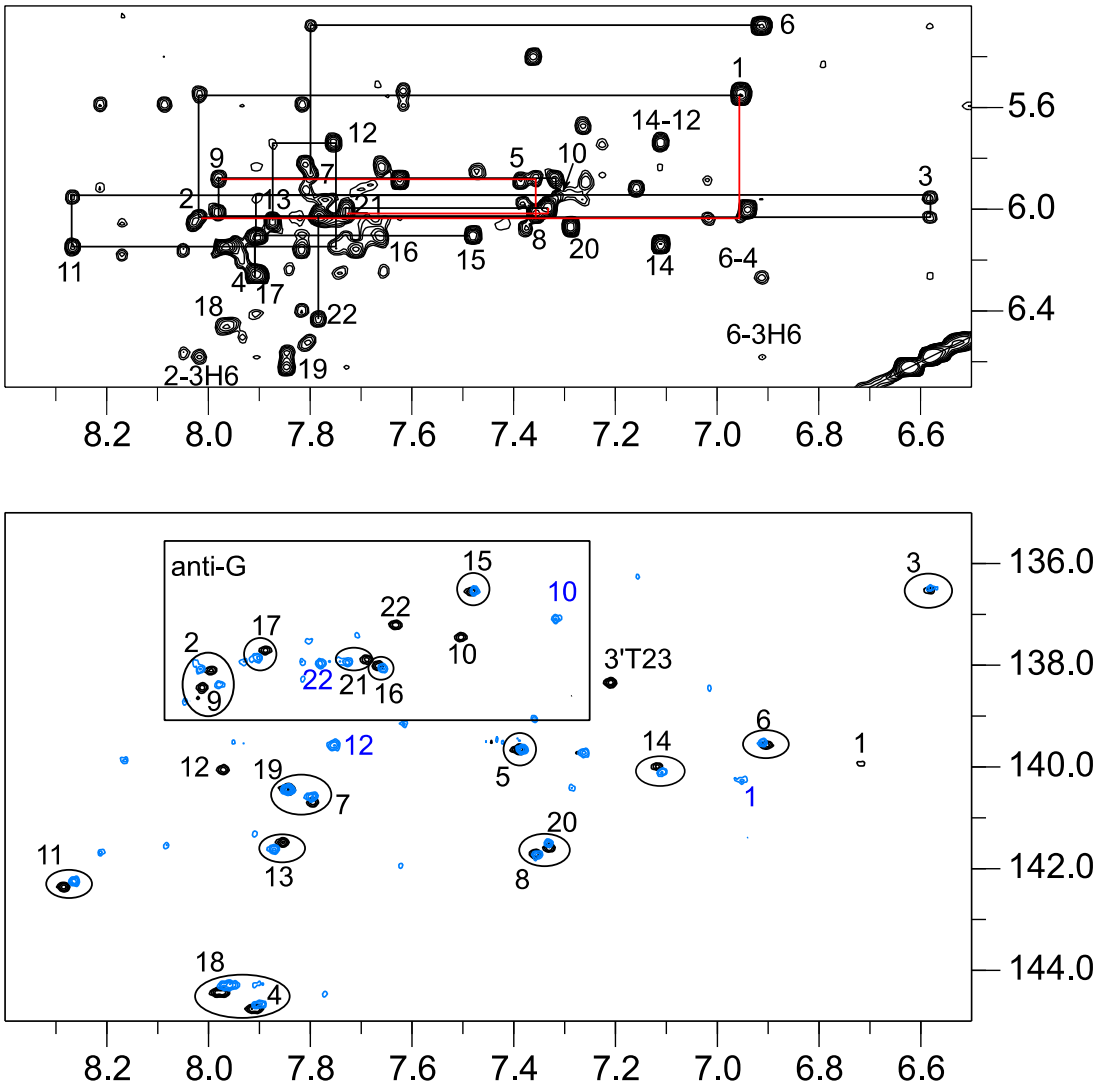

Figure S2. Partial assignment of *KNA-ΔG13*; 2D NOESY spectral region showing H6/8(ω_2)-H1'(ω_1) cross-peaks (top). Superimposed ^{1}H-^{13}C HSQC spectra with H6/8-C6/8 correlations of *KNA-ΔG13-T* (black, 0.9 mM) and *KNA-ΔG13* (blue) (bottom). Overlapping cross-peaks and cross-peak patterns suggest identical G4 topologies.

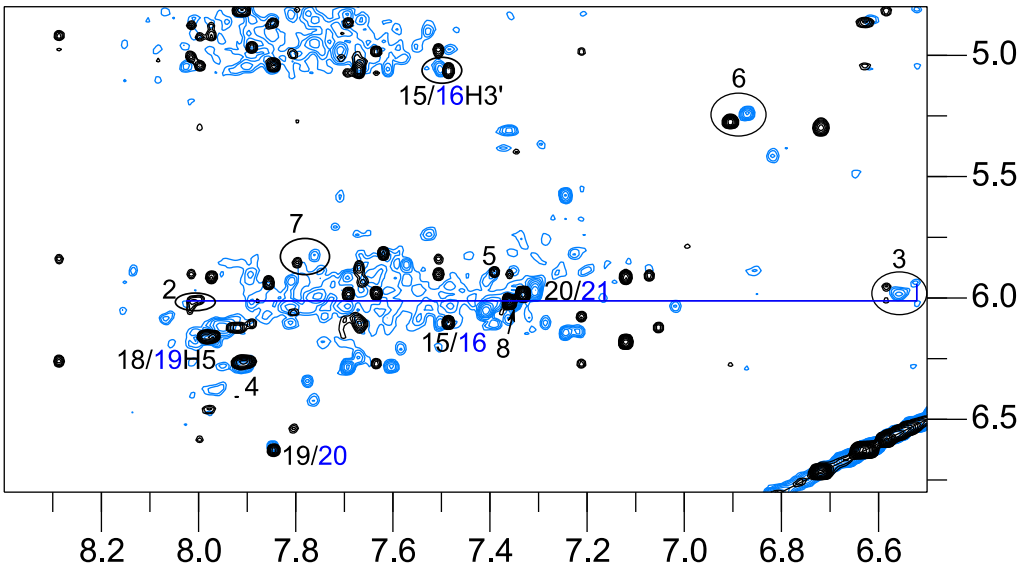

Figure S3. Partial assignment of *KNA-GGT*; superimposed 2D NOESY spectral region showing H6/8(ω_2)-H1'(ω_1) cross-peaks of *KNA-ΔG13-T* (black) and *KNA-ΔG13* (blue); several typical cross-peaks overlap, suggesting identical G4 topologies with assignments based on the *KNA-ΔG13-T* quadruplex.

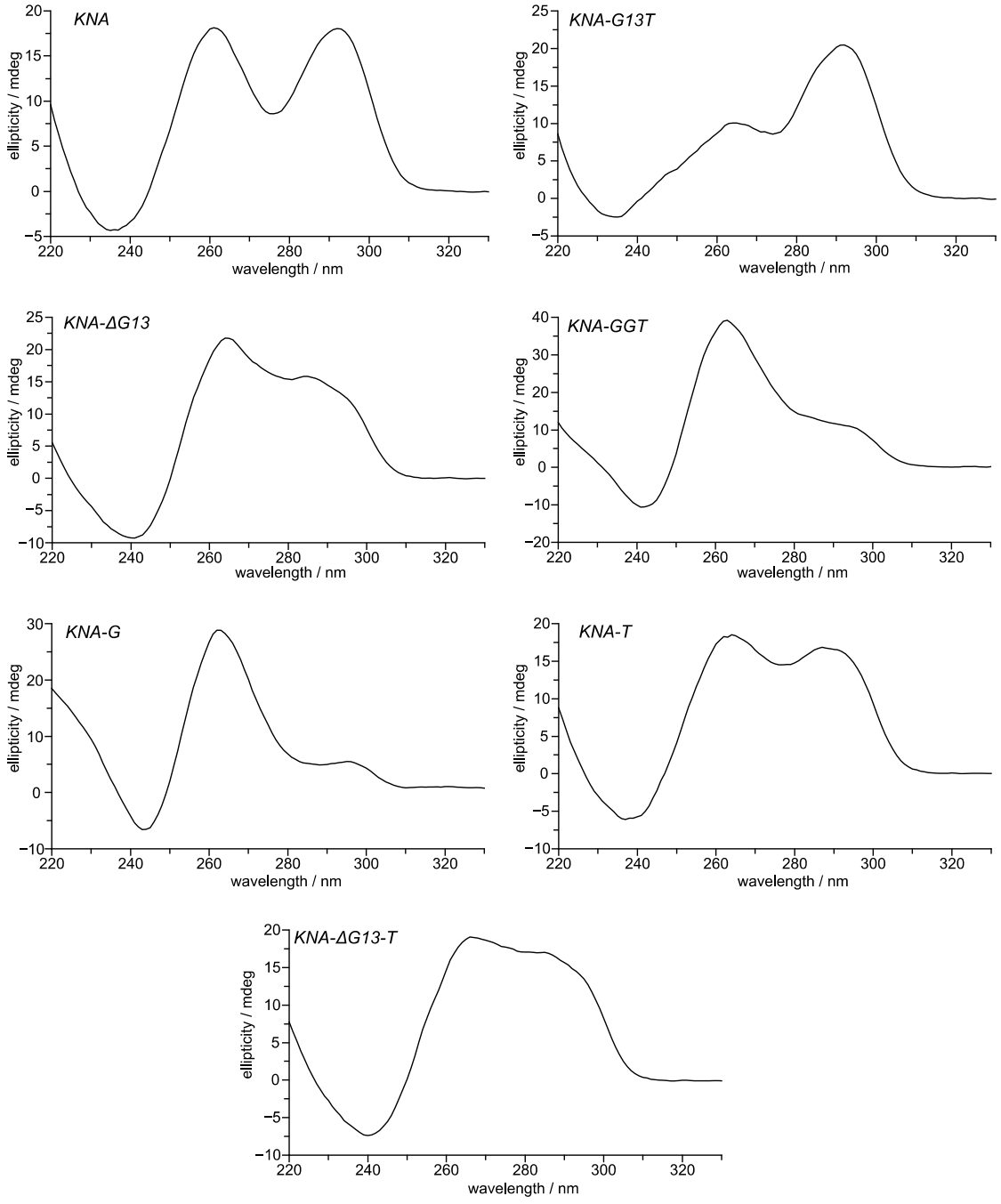

Figure S4. CD spectra of *KNA* variants at 20 ºC in 10 mM potassium phosphate buffer, pH 7.

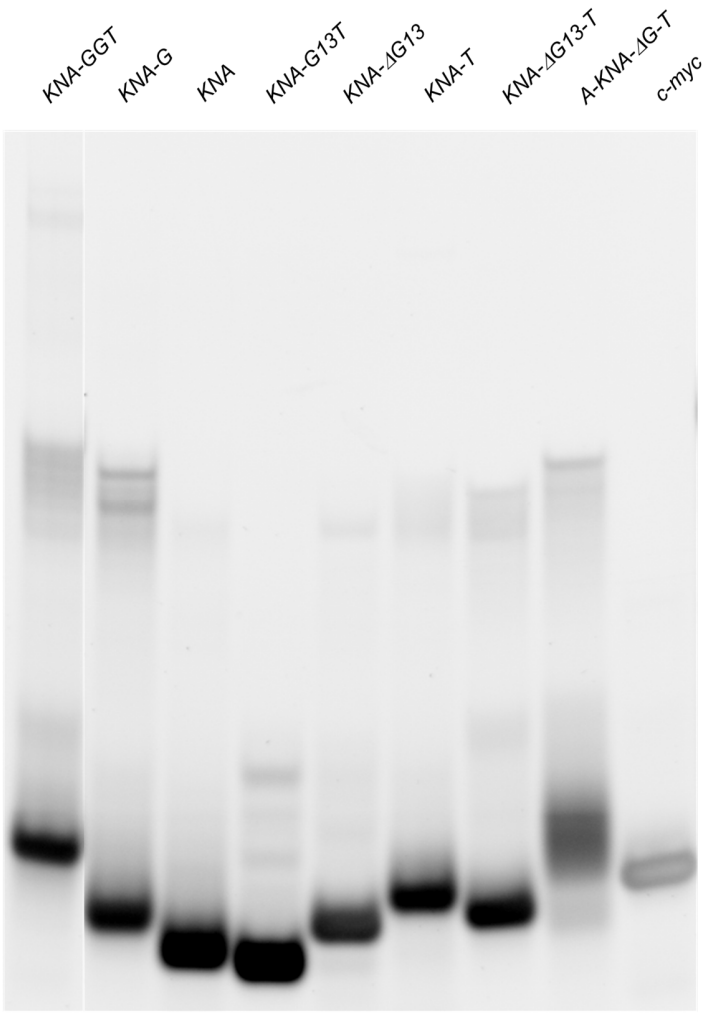

Figure S5. Non-denaturing gel electrophoresis of *KNA* variants and of a parallel 22mer *c-myc* quadruplex as additional reference. Slowly migrating weak bands are indicative of multimeric structures. Experimental procedure: **5**0 μM of annealed oligonucleotide samples in a 10 mM potassium phosphate buffer, pH 7.0, were mixed with glycerol-buffer (4:6) in a 1:1 v/v ratio. Samples (250 pmol per lane) were loaded on a 15% polyacrylamide gel (acrylamide:bis-acrylamide 19:1). Separation was performed in TBE buffer, pH 8.3, supplemented with 10 mM KCl. Gels were stained with 5 μM thiazole orange.

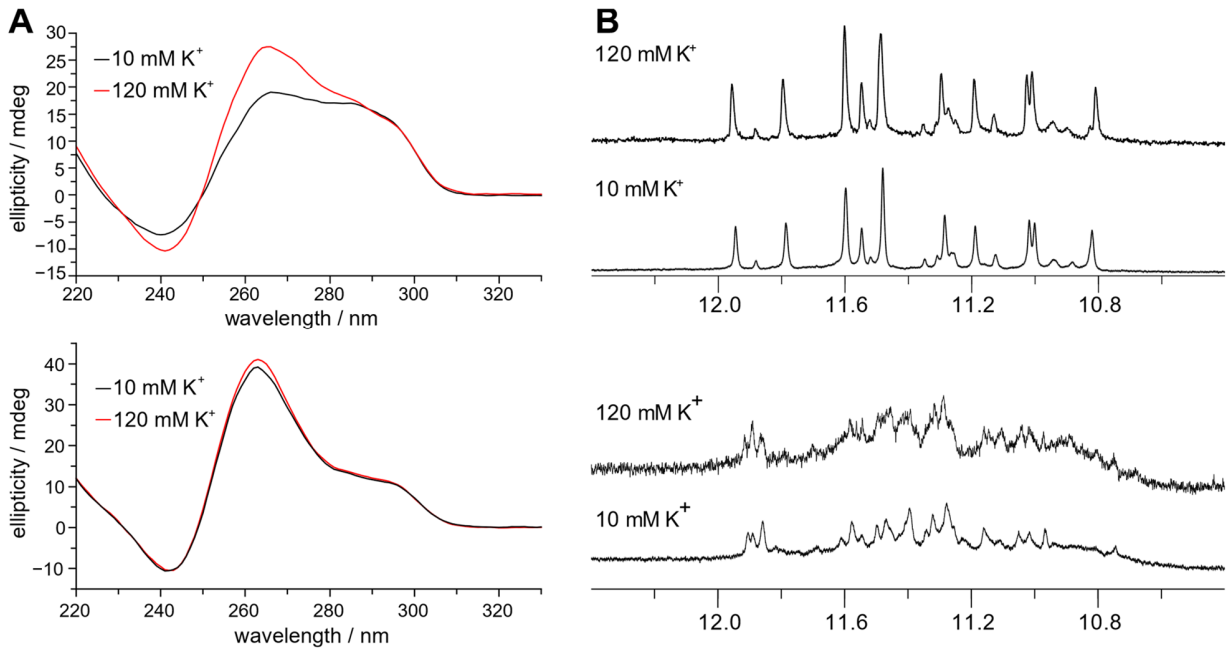

Figure S6. (A) CD spectra and (B) imino proton NMR spectral regions of *KNA-ΔG13-T* (top) and the *KNA-GGT* wild-type sequence (bottom) in buffer solutions with 10 mM and 120 mM K^+.

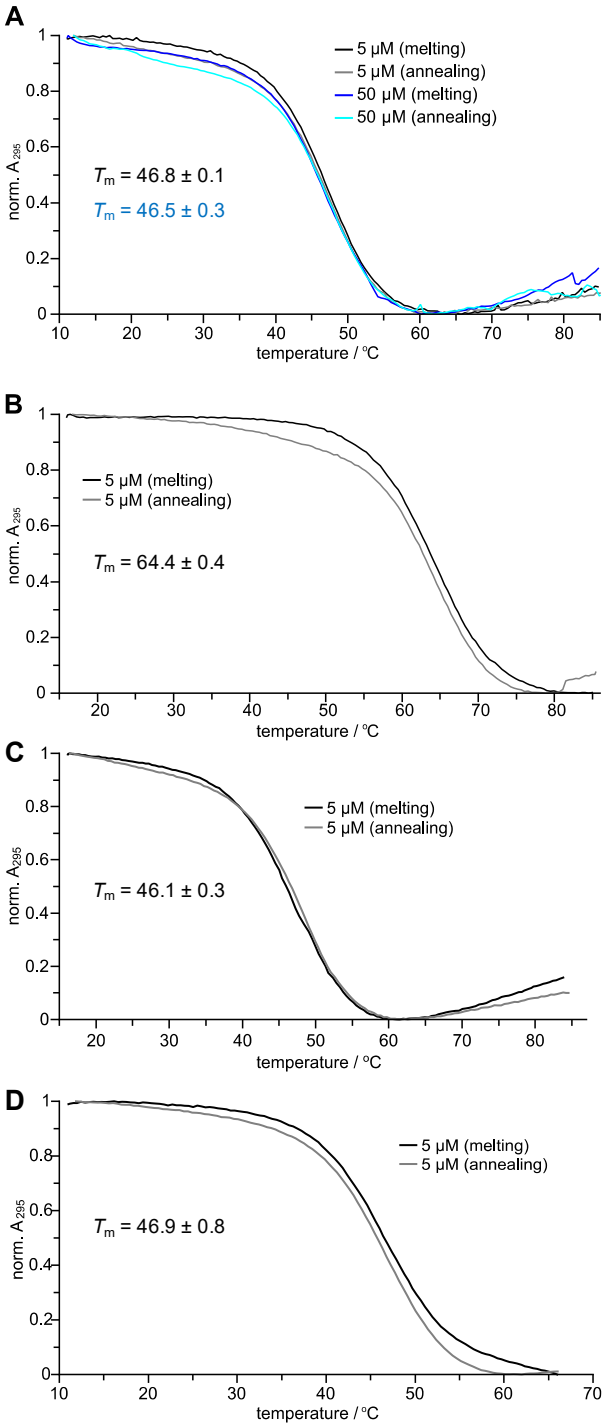

Figure S7. Representative UV melting curves. *KNA-ΔG13-T* in the presence of (A) 10 mM K^+ and (B) 120 mM K^+; (C) *KNA-ΔG13* and (D) *KNA-GGT* in the presence of 10 mM K^+; melting temperatures T_m are averages from three independent heating curves with standard deviations.

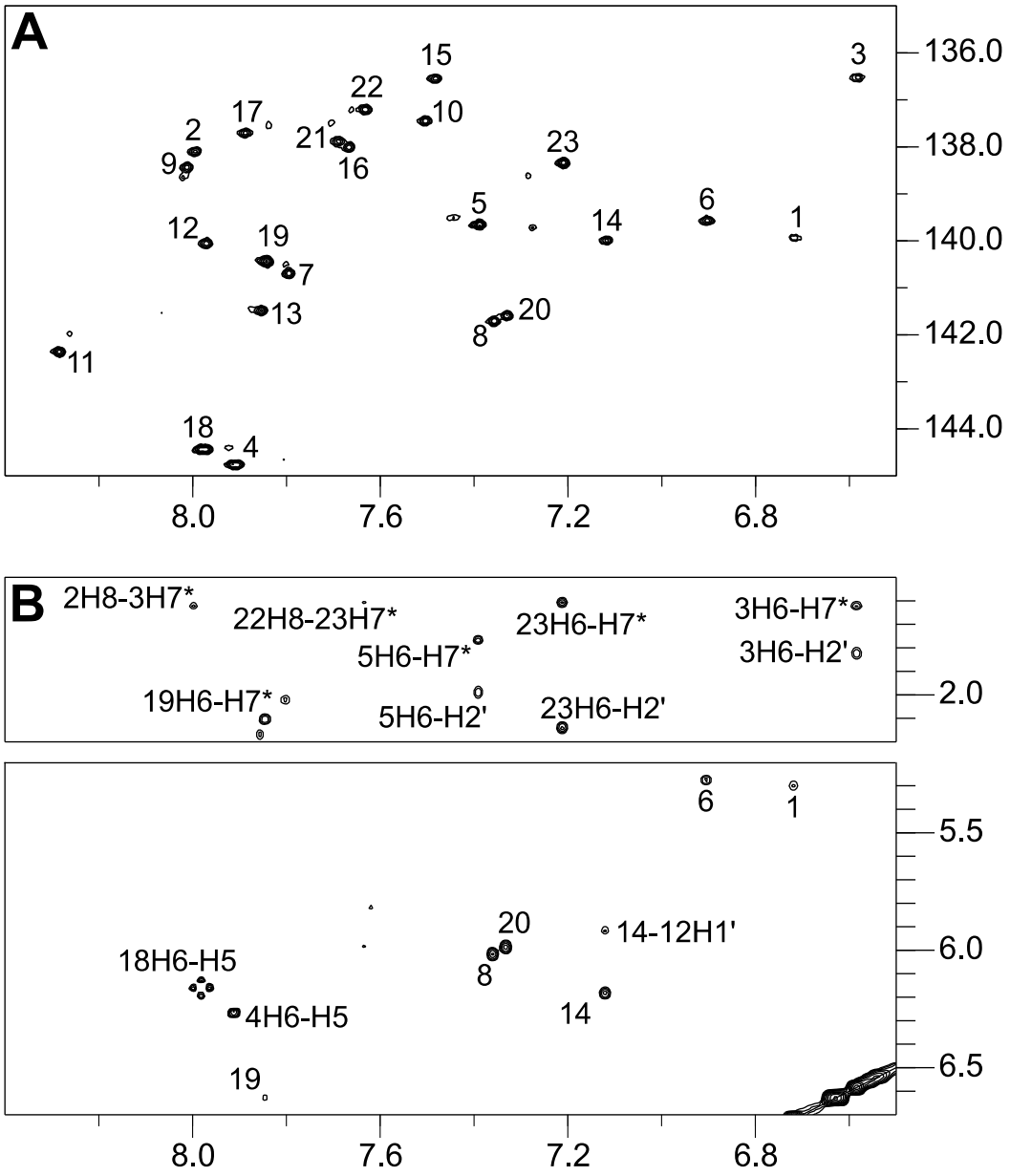

Figure S8. (A) H8/H6(ω_2)-C8/C6(ω_1) HSQC spectral region of *KNA-ΔG13-T* (0.94 mM) in a 10 mM K^+ buffer. (B) H8(ω_2)-H2'/Me(ω_1) (top) and H8(ω_2)-H1'(ω_1) spectral region (bottom) of a 2D NOESY spectrum of *KNA-ΔG13-T* acquired with an 80 ms mixing time at 25 °C in a 10 mM K^+ buffer.

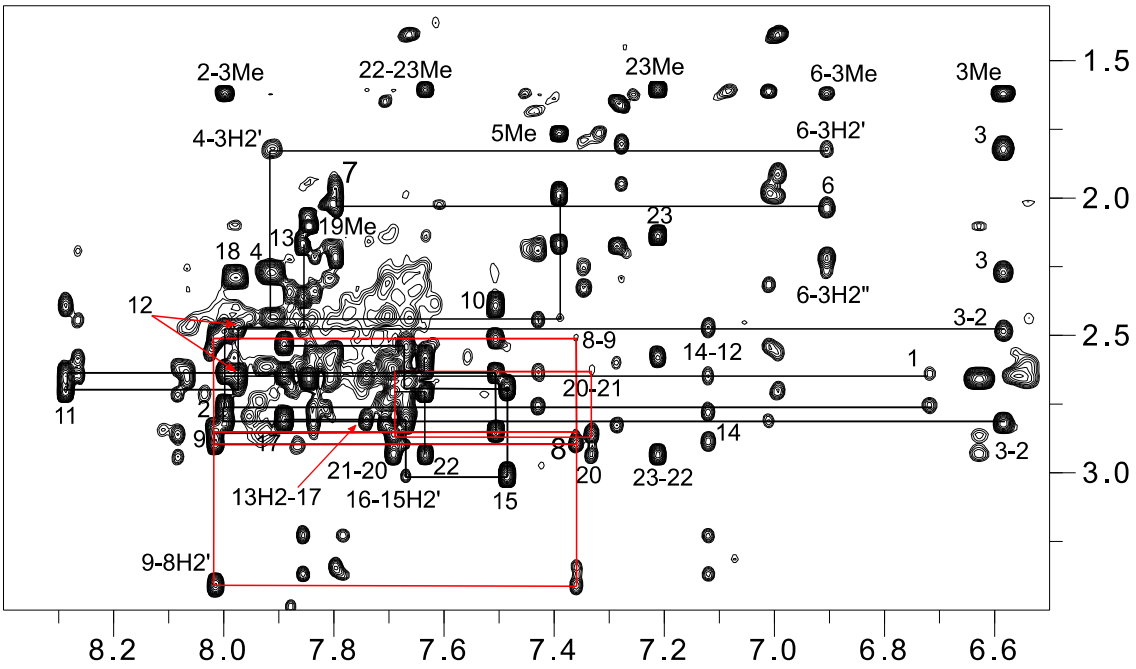

Figure S9. H8/H6(ω_2)-H2'/H2"/Me(ω_1) 2D NOESY spectral region of *KNA-ΔG13-T* (0.9 mM) acquired with a 300 ms mixing time; rectangular cross-peak patterns characteristic for *syn-anti* steps are colored red; the first residue number refers to H8/H6 resonances along ω_2.

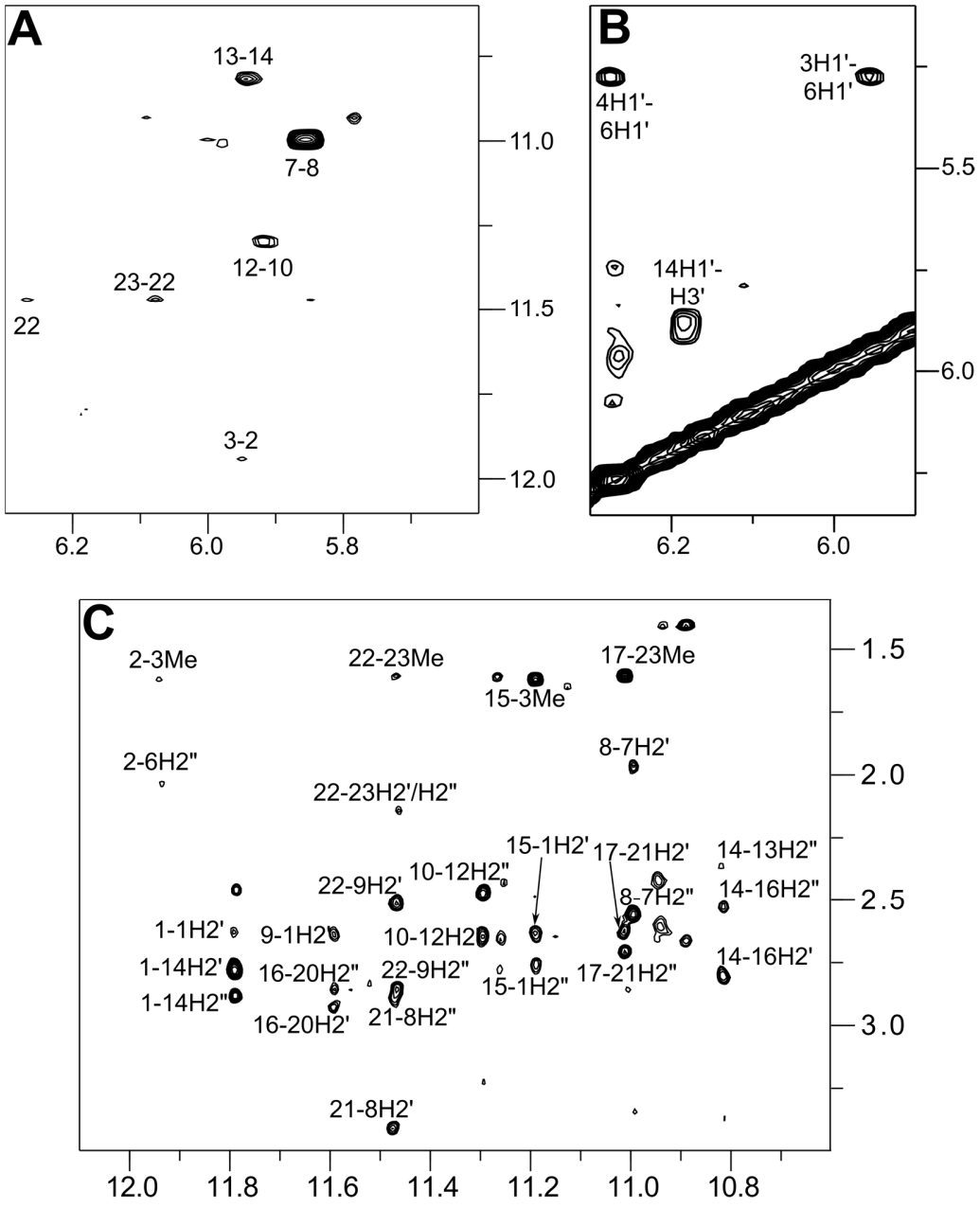

Figure S10. 2D NOESY spectrum of *KCNN4-ΔG13-T* (0.9 mM, 300 ms mixing time). (A) H1'(ω_2)-H1(ω_1) spectral region; (B) H1'(ω_2)-H1'/H3'(ω_1) cross-peaks within the first lateral loop; based on inter-residual H1'-H1' contacts, G6 is positioned close to T3 and C4; the unusually downfield-shifted G14 H3' resonance is also shown; (C) H1(ω_2)-H2'/H2"/Me(ω_1) spectral region; an NOE cross-peak between G9 H1 and G1 H2' indicates their opposite sugar-phosphate orientation.

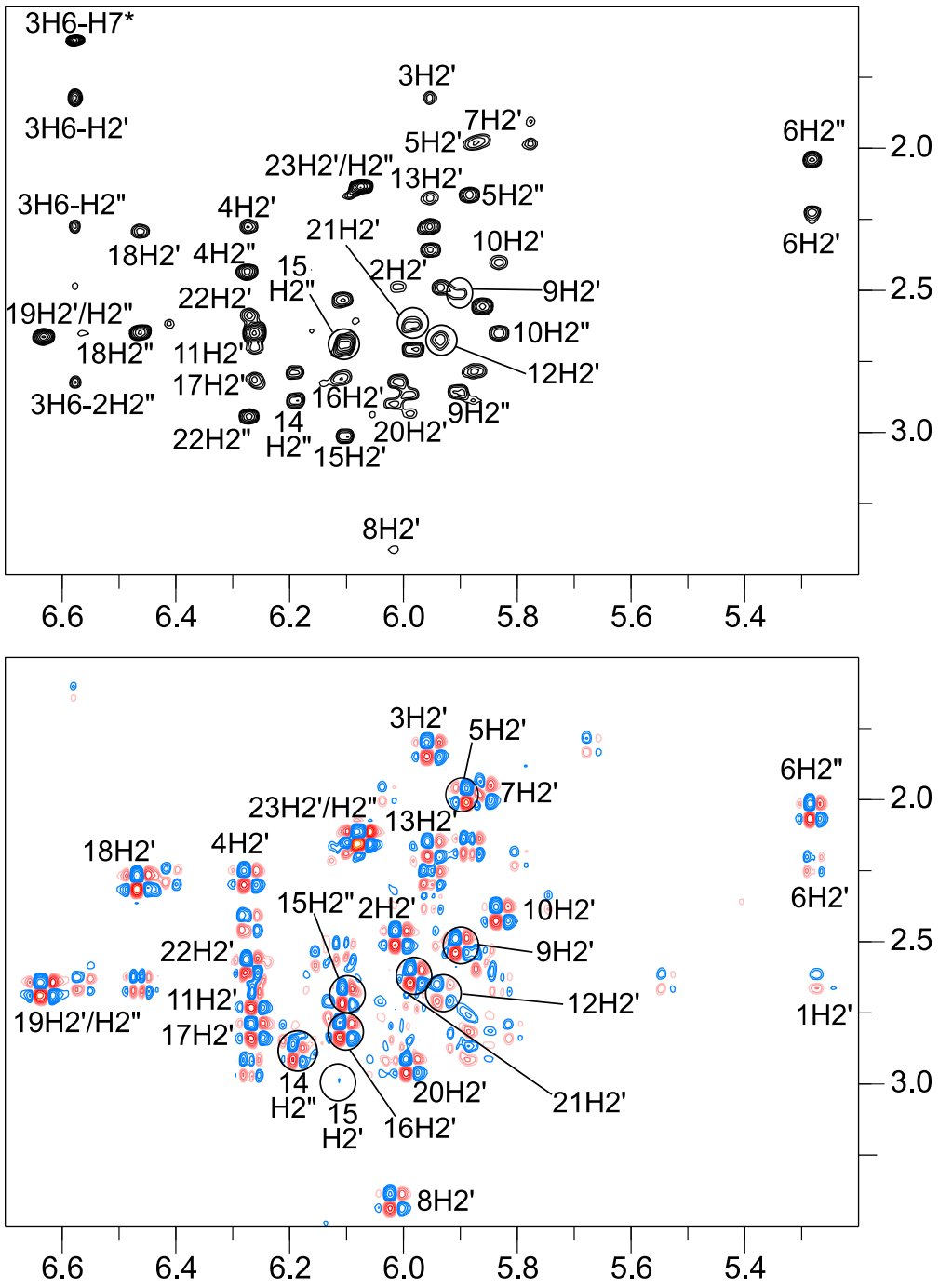

Figure S11. Determination of the sugar conformation. (A) Portion of a 2D NOESY spectrum (mixing time 80 ms) and (B) DQF-COSY spectral region of *KNA-ΔG13-T* (0.9 mM) in 100% D_2O showing H1'(ω_2)-H2'/H2"(ω_1) cross-peaks.

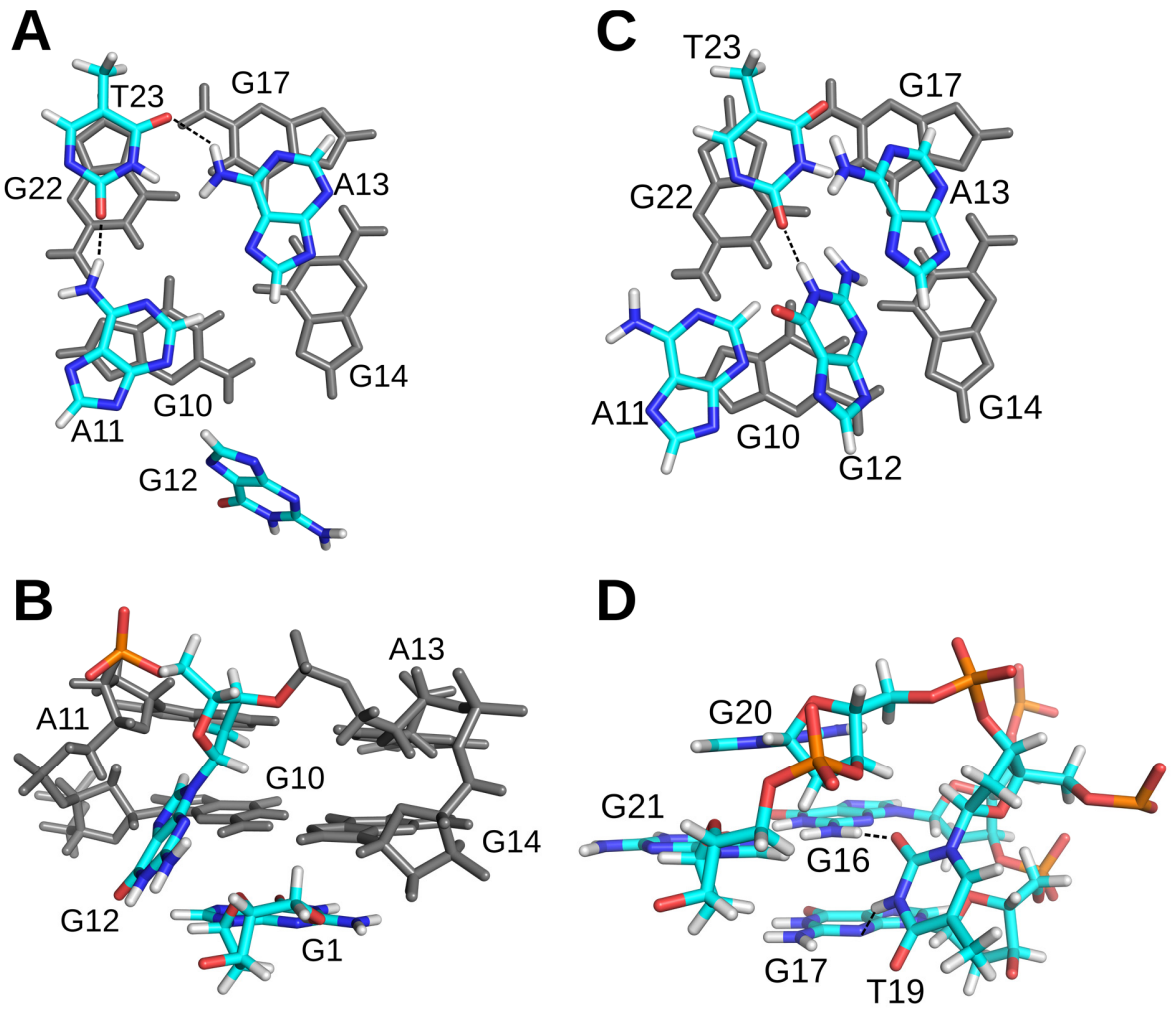

Figure S12. (A,B) Representative model of *KNA-ΔG13-T* with an orientation of the second lateral loop preceding the V-shaped loop as found in 8 out of 10 calculated structures. (A) Top view onto the second lateral loop and adjacent tetrad, highlighting a putative ATA triad between adenine bases of the lateral loop and 3'-terminal thymine T23. (B) Side view, highlighting G12 positioned nearly orthogonally to G1. (C) Top view onto the second lateral loop and adjacent tetrad, highlighting an alternative hydrogen bond formation between guanine G12 in the lateral loop and the 3'-terminal T23; tetrads are colored grey. (D) Putative hydrogen bond formation between the G16 amino proton and T19 O2 as well as between G17 N3 and T19 H3 of the propeller loop; C18 has been omitted for clarity.

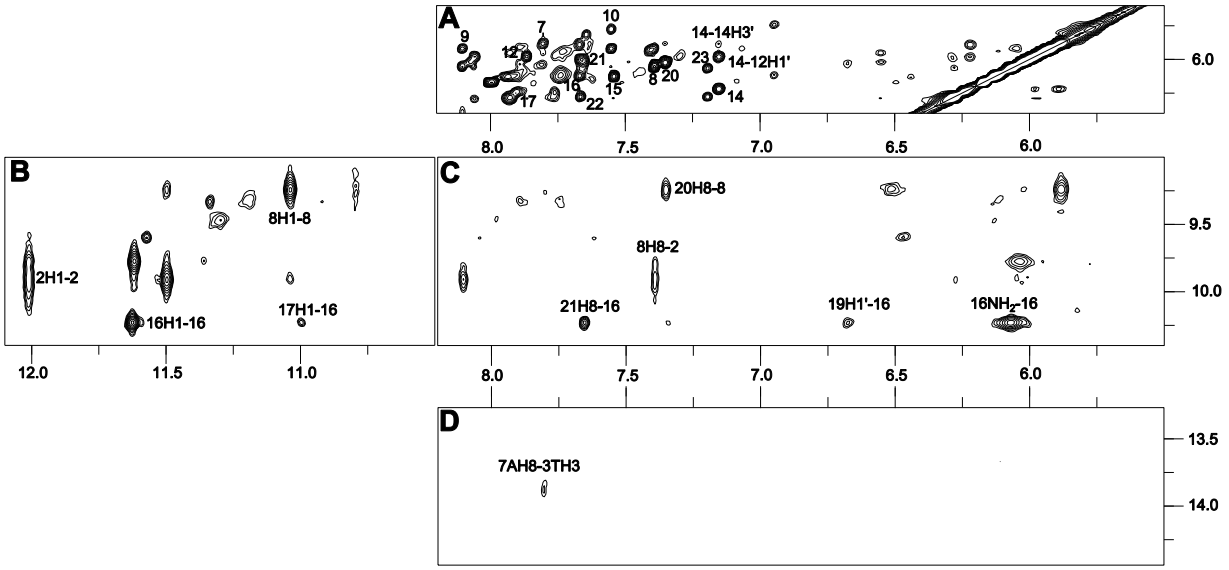

Figure S13. Portions of a 2D NOESY spectrum of *KNA-ΔG13-T* (0.9 mM, 300 ms mixing time, 278 K). (A) H6/8(ω_2)-H1'(ω_1) spectral region, (B) H1(ω_2)-amino proton(ω_1) spectral region, (C) H8/H1'/amino proton(ω_2)-amino proton(ω_1) spectral region. (D) Cross-peak which hints to the formation of an AT Hoogsteen hydrogen bond within the first lateral loop. Cross-peaks observed in this low-temperature spectrum were not included in the NOE-based distance restraints.

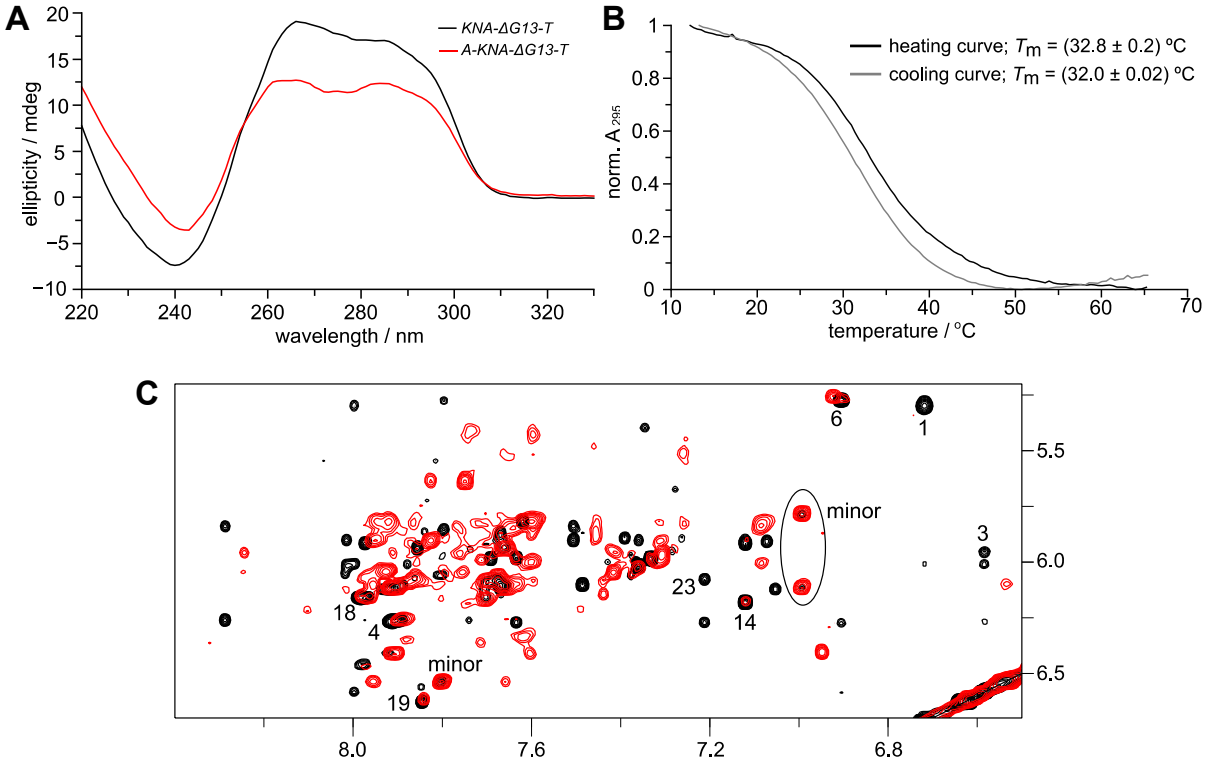

Figure S14. (A) CD spectrum of *A-KNA-ΔG13-T* (red) and *KNA-ΔG13-T* (black) in 10 mM K^+ buffer. (B) UV melting and annealing curves of *A-KNA-ΔG13-T* in 10 mM K^+ buffer with very small hysteresis effects. (C) Superposition of 2D NOESY spectra for *A-KNA-ΔG13-T* (red) and *KNA-ΔG13-T* (black) showing H6/8(ω_2)-H1'(ω_1) cross-peaks; labeled cross-peaks identify proton resonances of the V-shaped loop topology. Cross-peaks of the minor species coexisting with the V-shaped loop topology of *KNA-ΔG13-T* become more intense for *A-KNA-ΔG13-T* with a 5'-A overhang (circled); spectra were acquired at 25 ºC.

Table S1. ^{1}H and ^{13}C chemical shifts (in ppm) of *KNA-ΔG13-T* (0.9 mM) at 25 °C in 10 mM potassium phosphate buffer, pH 7.

Residues	H6/H8	H2/5/Me	H1	H1'	H2'	H2"	H3'	C6/8	C5	C2
G1	6.72	-	11.79	5.30	2.64	2.76	4.93	139.93	119.59	-
G2	8.00	-	11.94	6.01	2.49	2.82	5.05	138.10	117.48	-
T3	6.58	1.62	-	5.96	1.82	2.27	4.82	136.53	-	-
C4	7.91	6.27	-	6.27	2.28	2.44	4.81	144.76	-	-
T5	7.39	1.77	-	5.89	2.28	2.44	4.81	139.67	-	-
G6	6.91	-	-	5.28	2.22	2.04	4.64	139.56	-	-
A7	7.80	7.22	-	5.85	1.97	2.56	4.81	140.71	-	153.44
G8	7.36	-	11.00	6.01	3.41	2.90	4.88	141.71	119.82	-
G9	8.01	-	11.59	5.90	2.51	2.85	5.01	138.44	116.84	-
G10	7.51	-	11.30	5.84	2.40	2.64	4.98	137.45	117.09	-
A11	8.29	7.78	-	6.26	2.70	2.65	4.92	142.36	-	154.54
G12	7.97	-	-	5.92	2.65	2.48	4.88	140.07	-	-
A13	7.86	7.74	-	5.94	2.17	2.36	4.72	141.49		154.25
G14	7.12	-	10.82	6.18	2.78	2.89	5.88	140.00	118.77	-
G15	7.49	-	11.19	6.10	3.01	2.70	5.07	136.56	118.24	-
G16	7.67	-	11.59	6.11	2.81	2.54	4.97	138.01	117.10	-
G17	7.89	-	11.01	6.26	2.81	2.65	4.97	137.72	117.66	-
C18	7.98	6.16	-	6.46	2.29	2.65	4.62	144.44	-	-
T19	7.84	2.10	-	6.63	2.66	2.66	5.04	140.44	-	-
G20	7.33	-	11.56	5.99	2.93	2.86	4.87	141.60	119.61	-
G21	7.69	-	11.47	5.98	2.63	2.71	5.08	137.89	116.77	-
G22	7.63	-	11.47	6.27	2.58	2.94	4.98	137.21	117.50	-
T23	7.21	1.61	-	6.08	2.14	2.14	4.51	138.35	-	-